

## THE VARIABLE WARM ABSORBER IN CIRCINUS X-1

N. S. SCHULZ<sup>1</sup>, T. E. KALLMAN<sup>2</sup>, D. K. GALLOWAY<sup>3</sup>, AND W. N. BRANDT<sup>4</sup>

*accepted for publication September 4, 2007 by The Astrophysical Journal*

### ABSTRACT

We observed Circinus X-1 twice during a newly reached low-flux phase near zero orbital phase using the High-Energy Transmission Grating Spectrometer (HETGS) onboard *Chandra*. In both observations the source did not show the P Cygni lines we observed during the high-flux phases of the source in 2000 and 2001. During pre-zero phase the source did not exhibit significant variability and exhibited an emission-line spectrum rich in H- and He-like lines from high Z elements such as Si, S, Ar, and Ca. The light curve in the post-dip observation showed quiescent and flaring episodes. Only in these flaring episodes is the source luminosity significantly higher than observed during the pre-zero phase. We analyzed all high resolution X-ray spectra by fitting photoionization and absorption models from the most recent version of the XSTAR code. The pre-zero phase spectrum could be fully modeled with a very hot photoionized plasma with an ionization parameter of  $\log \xi = 3.0$ , down from  $\log \xi = 4.0$  in the high-flux state. The ionization balances we measure from the spectra during the post-zero phase episodes are significantly different. Both episodes feature absorbers with variable high columns, ionization parameter, and luminosity. While cold absorption remains at levels quite similar to the one observed in previous years, the new observations show unprecedented levels of variable warm absorption. The line emissivities also indicate that the observed low source luminosity is inconsistent with a static hot accretion disk corona (ADC), an effect that seems common to other near edge-on ADC sources as well. We conclude that unless there exists some means of coronal heating other than X-rays, the true source luminosity is likely much higher and we observe obscuration in analogy to the extragalactic Seyfert II sources. We discuss possible consequences and relate cold, luke-warm, warm, and hot absorbers to dynamic accretion scenarios.

*Subject headings:* stars: individual (Cir X-1) — stars: neutron — X-rays: stars — binaries: close — accretion: accretion disks — techniques: spectroscopic

### 1. INTRODUCTION

Not many X-ray binaries show as large a variety of X-ray features and properties as Circinus X-1. Since its discovery (Margon et al. 1971), this X-ray binary has appeared at various X-ray brightness levels ranging from only a few to several hundreds of mCrab (Parkinson et al. 2003). Its long-term brightness featured flaring activity at increasing levels during the 1970s and 1980s and a steady increase in overall brightness during the 1990s until at some point it reached a flux of about 1.5 Crab. The discovery of broad P Cygni line profiles during these bright periods (Brandt & Schulz 2000; Schulz & Brandt 2002) demonstrated the presence of a high-velocity outflow likely in the form of an accretion disk wind. The simultaneous presence of possibly relativistic jets (Fender et al. 1998, 2004a) underlines the highly violent nature of the source at the time.

Since then Cir X-1 has calmed considerably in its X-ray emission and although the X-ray light curve still shows its characteristic pattern with an orbital period of 16.6 days (Kaluzienski et al. 1976), its outbursting power near zero phase also has diminished to only a fraction of the levels it showed a few years ago. In recent months the source was only barely or not detected with the *RXTE*

ASM (Jonker et al. 2007a). In most respects the nature of Cir X-1 is still poorly understood. Despite advances in recent years, there remains uncertainty about even the most basic properties of this system. Recent observations of quasi-periodic oscillations (QPOs) added more incentives to a long list of indirect evidence that the compact object in Cir X-1 is in fact a neutron star (Shirey et al. 1999; Tennant et al. 1986; Qu et al. 2001; Tauris et al. 1999; Boutloukos et al. 2006). Some new insights on the nature of its companion came from a recent analysis by Jonker et al. (2007b) who argue for an earlier A to late B-type star. Moneti (1992) had detected a heavily reddened optical counterpart with strong, asymmetric and variable H $\alpha$  emission (Whelan et al. 1977; Mignani et al. 1997; Johnston et al. 2001).

The system's orientation has become a much debated issue (Schulz et al. 2006). Perhaps one of the most exciting but also controversial features of Cir X-1 is the existence of a possibly ultrarelativistic radio jet. Under the assumption that the jet was launched during the most recent periastron passage, Fender et al. (2004a) deduce an upper limit to the inclination of about 11°. Most recent projections of orbital parameters postulate an angle of no less than 14° (Jonker et al. 2007b). Recently Heinz et al. (2007) found evidence for a parsec scale X-ray jet from Cir X-

<sup>1</sup>Kavli Institute for Astrophysics and Space Research, Massachusetts Institute of Technology, Cambridge, MA 02139.

<sup>2</sup>Goddard Space Flight Center, NASA, Greenbelt, MD.

<sup>3</sup>School of Physics, University of Melbourne, Parkville 3010, Australia.

<sup>4</sup>Department of Astronomy & Astrophysics, 525 Davey Laboratory, The Pennsylvania State University, University Park, PA, 16802.

1 which also appears consistent with some lower inclination for an unbended jet. X-ray spectral studies do not directly provide evidence about inclination since no eclipses are observed. However, extensive studies with *ASCA* and *RXTE* (Brandt et al. 1996; Shirey et al. 1999), and later with *Chandra* (Brandt & Schulz 2000; Schulz & Brandt 2002) produced arguments for a highly inclined viewing angle including an equatorial wind-like outflow that now seems to be a quite typical property of these types of X-ray binaries (Blundell et al. 2001; Miller et al. 2006a,b).

In this respect Circinus X-1 belongs to a now long list of Galactic microquasars Mirabel (2001) named in analogy to their extragalactic cousins, the Seyfert galaxies. One of the trademarks of active galactic nuclei is, besides an X-ray bright nucleus and prominent relativistic jets, the existence of warm absorbers. There are various types of X-ray absorbers in X-ray sources. Widely known in Galactic X-ray binaries is photoelectric absorption due to cool and lowly ionized matter of the interstellar medium (Morrison & McCammon 1983; Wilms et al. 2000; Paerels et al. 2001; Juett et al. 2004, 2006) as well as circumstellar and circumdisk material (Watanabe et al. 2003; Schulz et al. 2002a; Juett et al. 2006). The most prominent indication for the existence of large amount of such cool circumstellar material is the existence of significant line fluorescence as well orbitally correlated column densities. The existence of Seyfert-like warm absorber outflows in microquasars other than Cir X-1 has recently also been observed with *Chandra* in GX 339-4 and GROJ 1655-40 (Miller et al. 2004, 2006b). The term warm absorber was introduced during the mid-1980s by Halpern (1984) as an illuminated plasma of moderate electron temperature ( $< 10^7$  K) which shows similar levels of ionization as a collisionally ionized hot gas. Quite impressive examples of warm absorbers have been shown for AGNs like MCG 6-30-15 (Lee et al. 2002) and NGC 3783 (Kaspi et al. 2002). A recent overview of warm absorber properties in AGN was given by Blustin et al. (2005).

In this third paper, we present results from two new observations of the Galactic microquasar Circinus X-1 performed during a phase where the source was at an overall extremely low flux level. As in papers I and II (Brandt & Schulz 2000 (BSI) and Schulz & Brandt 2002 (SBII)) the observations were performed with the High-Energy Transmission Grating Spectrometer (HETGS) on-board *Chandra* at “zero phase.” Zero phase in Cir X-1 is thought to be associated with the periastron passage of the neutron star. The observations include a shorter exposure during the pre-zero phase dip and a longer exposure at zero phase where the source usually exhibits strong variability. The second of these observations was also the basis for the discovery of the parsec-scale X-ray jet by Heinz et al. (2007). Throughout this paper, we adopt a distance to Cir X-1 of 6 kpc (Stewart et al. 1993; Case et al. 1998) and an interstellar column density of about  $2 \times 10^{22} \text{ cm}^{-2}$  (e.g., Predehl & Schmitt 1995).

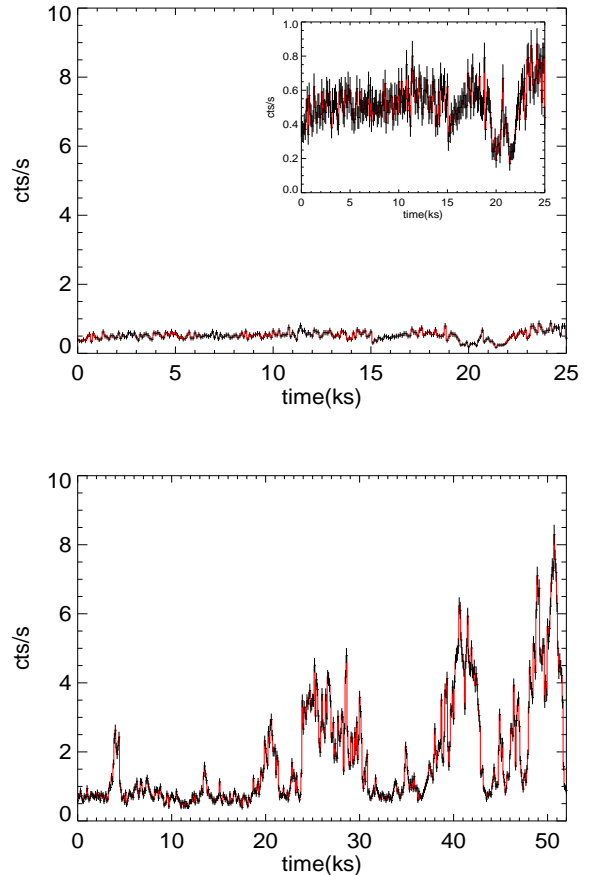


FIG. 1.— The light curves of obs. III (top) and IV (bottom). The data were binned by adding all HETG 1st order photons from 1.6 to 10 Å. The y-scale of the two curves was kept the same for better comparison. The inset in the top image shows a blow up of III.

## 2. CHANDRA OBSERVATIONS

Cir X-1 was observed with the HETGS (see Canizares et al. 2005 for a detailed description) on 2005 January 3 (starting at 01:14:52 UT) for 25 ks (observation III, OBSID 6148) and on 2005 June 2 (starting at 23:44:51 UT) for another 50 ks (observation IV, OBSID 5478). The denominations ‘III’ and ‘IV’ stem from the fact that we observed Cir X-1 a few years earlier in a very similar manner and instrument configuration which were labeled as observations I and II (SBII). Both observations were performed near zero phase of the binary orbit. Observation III was performed during an often occurring pre-zero phase dip at phase 0.96 – 0.99, while obs. IV occurred a few phase bins later at phases 1.06 – 1.10 (adopting the ephemeris of Glass 1994). Both observations were configured the same way. The detector array (ACIS-S) consists of 6 CCDs which were clocked choosing a 512 pixel row subarray placed near the readout in order to reduce the frame time to about 1.7 s. There were two distinct differences in the setup of the two observations which stemmed from two erroneous settings during obs. III. While the first produced a different off-axis angle of the telescope with the only consequence that chip gaps in the effective area fall into different wavelength bands, the second was a bit more costly. Due to an incorrectly placed exclusive count window filter on the central CCD (and we detect no source

TABLE 1: CHANDRA HETGS X-RAY OBSERVATIONS IN 2005

Obsid	label	Start Date [UT]	Start Time [UT]	Exposure [ks]	HEG -1st rate cts s <sup>-1</sup>	Phase range
6148	III	Jan 03 2005	01:14:52	24.48	0.228	0.96 – 0.99
5478	IV	Jun 02 2005	23:44:51	51.62	0.524	1.06 – 1.10

photons above 10 Å), the spectra in obs. III possess only about 50% of the anticipated exposure.

All observations were reprocessed using CIAO3.4 with the most recent CALDB products. In order to fine tune the wavelength scale we redetermined the zero-order position in both observations. For obs. IV we have a strong 0th order point source with read out trace and positive and negative order dispersion. This allows us to reach a positional accuracy of about 1/4 of a detector pixel ensuring a wavelength scale accuracy of about 1/8 of a resolution element, i.e. 0.0025 Å for MEG and 0.0015 Å for HEG spectra. In obs. III the 0th order was filtered for every 10th photon and weak, and due to the misplaced exclusion window we do not have a read out trace and significant negative order spectra. This severely limited our ability to determine a precise 0th order position. Therefore for obs. III we only reach an accuracy of 0.010 Å for MEG and 0.005 Å for HEG in our wavelength scale. For transmission gratings the dispersion scale is linear in wavelength and we perform the spectral analysis always in wavelength space to avoid non-linear binning. We used standard wavelength redistribution matrix files (RMF) but generated ancillary response files (ARFs) using the provided aspect solutions, bad pixel maps, and CCD window filters.<sup>5</sup> For all the observations we generated spectra and analysis products for the 1st orders only.

Figure 1 shows the light curves of the two observations. Note that since obs. III (top) occurred at pre-zero orbital phase, the count rate appears exceptionally low. However, even compared with observation II from the year 2000 at similar phase, the rate has dropped by over two orders of magnitude. Observation IV (bottom) shows not only the expected higher rate, but also quite significant variability. Besides episodes of relative quiescence the source now engages in frequent flares. Though this is not unexpected during this orbital phase, the observed activity has a somewhat different appearance compared to the activity in previous years where the flux rose rather quickly to a high level accompanied by many dipping episodes (e.g., Shirey et al. 1999). Compared to the flux levels in previous years, this rate of the source even in this phase is now quite moderate and also reduced by almost two orders of magnitude.

### 2.1. Continuum Spectra and Fluxes

In order to determine the source flux during the two exposures we fit the source spectra with generic continuum models. Unlike in obs. I and II, where we had severe spectral degradation due to photon pileup, we do not have to restrict ourselves to specific spectral ranges or rely on

higher orders in our new observations. While obs. III is practically pileup free, possible pileup at the maximum photon fluxes in obs. IV is below 2%, which we treat as a contribution to the systematic uncertainty. For the flux analysis we also exclude detected line features (see below) which although not significantly contributing to the overall source flux will affect the broad band continuum fit. The main motivation for this portion of the analysis is to obtain X-ray fluxes which serve as a check on the outcome of the fits using the detailed photoionization model below. We also investigate potential similarities of the continuum shape with previous observations.

Figure 2 indicates that there is no significant flux longward of 10 Å. This is different from the previous observations, where we have flux contributions up to 14 Å and use a model spectrum based on previous fits to ASCA data (Brandt et al. 1996) consisting of two blackbody components with both intrinsic partial-covering absorption in addition to interstellar absorption. The raw spectra in obs. III and IV indicate a high level of complexity involving a combination of emission and absorption. We could not produce good fits for both observations using the double partially covered blackbody model, but found similar options. Table 2 summarizes the fit results. Statistically only one simple power law plus absorption was required for observation III. This was not the case in obs. IV, which in order to include the softer end of the spectrum (i.e., above 5.2 Å) needed an additional component. Galloway et al. (2007) successfully fitted a single blackbody with partial coverage absorption to high flux spectra at higher orbital phases. The fits produced reduced  $\chi^2$  below 1.5 only under certain conditions. In obs. III the fit only allowed for interstellar absorption leaving significant residuals near the Si and Fe K edges. In observation IV the model fit only if the wavelength range was restricted to 2 – 8 Å.

The next step involved a two-component model consisting of two power laws, also with additional absorption. One of the components required significant additional absorption with a partial covering fraction above the 90% level. Substitutions of one of the components with blackbody functions left the reduced  $\chi^2$  well above 1. Still, the two-component configuration is relatively similar to what we found in observation I and II (SBII) and we therefore applied it to obs. III as well. We found a good fit with rather similar parameters. Here the substitution of the absorbed power law with a blackbody worked as well. The conclusion we draw from this is that the new spectral shape is likely not much different from the one in the high-flux states a few years ago. The models also suggest that the transition between pre- and post-zero phases

<sup>5</sup>see <http://asc.harvard.edu/ciao/threads/>

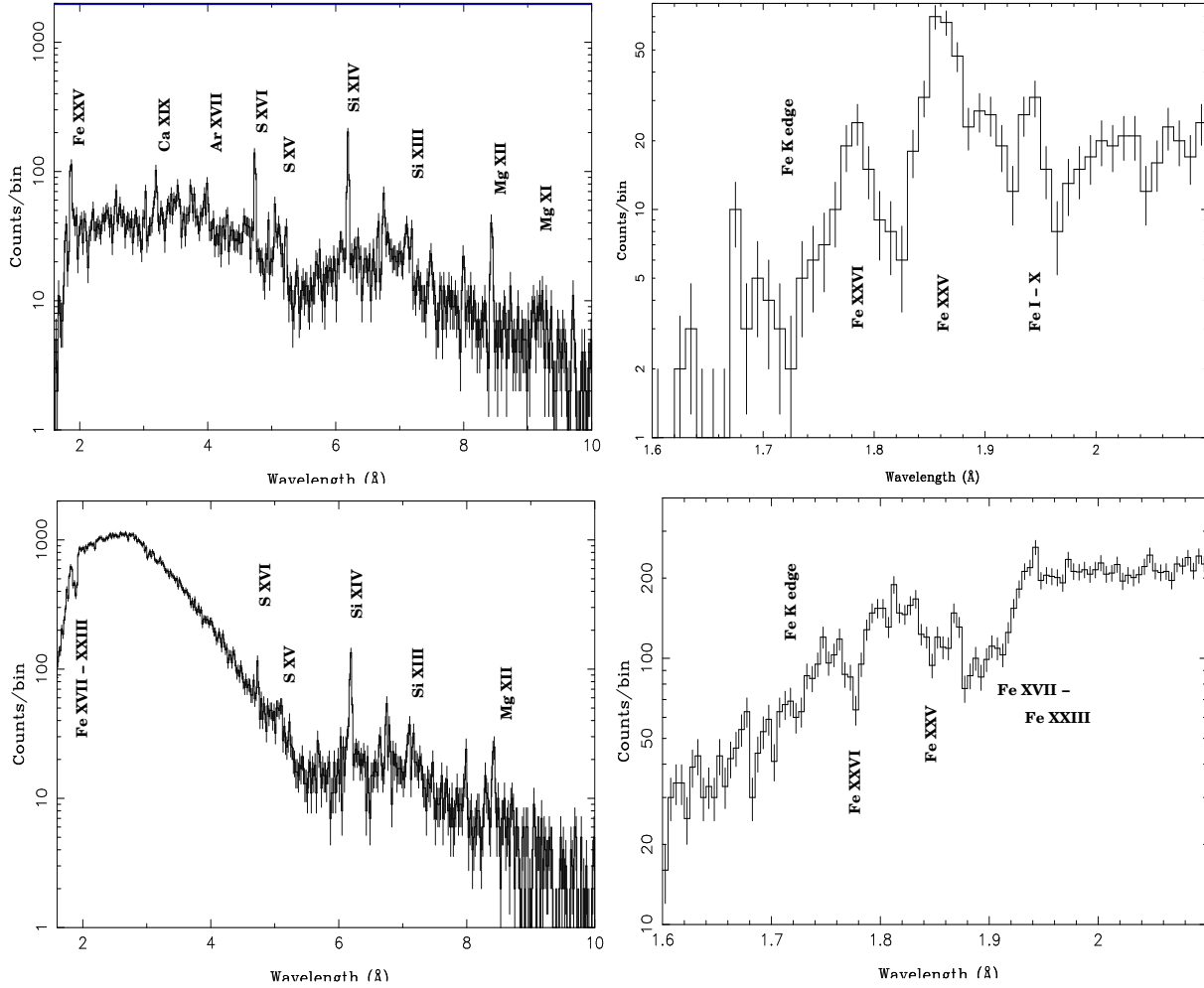


FIG. 2.— The raw spectra of obs. III (top) and IV (bottom) from all HETG 1st order photons. In both cases the spectral bandpass is limited to wavelengths below 10 Å indicating high column densities.

is predominantly a change in the hard absorbed spectral component. Most important, however, is the fact that the continuum is consistent with a power law shape in both, the hard and softer parts of the spectra, which then allows a relatively straightforward treatment of photoionization and -absorption. The absorbed source flux (2 – 10 keV) in obs. III was determined to  $(1.23 \pm 0.02) \times 10^{-10}$  erg cm $^{-2}$  s $^{-1}$  and in obs. IV was  $(5.72 \pm 0.03) \times 10^{-10}$  erg cm $^{-2}$  s $^{-1}$ . The interstellar column density is assumed to be  $1.94 \times 10^{22}$  cm $^{-2}$  as provided by many previous X-ray analyses and which is close to the predicted column from H I measurements in this line of sight (Predehl & Schmitt 1995). Both spectra in all models show that substantial additional absorption is required.

### 3. DETAILED SPECTRAL ANALYSIS

Our models for the spectral features (emission and absorption lines, and bound-free absorption) consist of both phenomenological fits, using Gaussian lines, and fits to photoionization models constructed using the XSTAR (v. 2.1ln2) code.<sup>6</sup> XSTAR calculates both the ionization/excitation of a gas illuminated by a strong source of X-rays and also the spectral features imprinted by the gas, both in emission and absorption. This is available as an ‘analytic’ model in XSPEC<sup>7</sup>, which can also be imported into ISIS.<sup>8</sup> The models assume a time-steady balance between processes affecting ionization, recombination, excitation, de-excitation, heating and cooling of the gas. The key parameters determining the emission and absorption properties are the shape of the incident spectrum and the ionization parameter, defined as  $\xi = 4\pi f_x / n_e$ , where X-ray flux  $f_x$  is defined as the energy flux incident on the gas integrated from 1 – 1000 Ry (Tarter et al. 1969) and  $n_e$  is the electron number density in the gas. Additional parameters include the elemental abundances, bulk velocity or redshift, and turbulent velocity, in addition to the column density or the emission measure for absorption or emission models, respectively. Each model component is idealized as a uniform medium with a given set of input parameters. Emission and absorption components can be combined, either singly or multiply, using standard ‘model’ commands in XSPEC or ISIS.

For all spectra we performed simultaneous fits to the individual 1st order spectra of the MEG and HEG. Only for plotting purposes are the spectra and model fits added together. During the analysis we binned the spectra into 0.005 Å bins which matches the available MEG bins and undersamples the HEG by a factor of 2.

#### 3.1. Emission Lines

Table 3 lists all detected lines with positions and fluxes obtained from Gaussian fits. The values were obtained by fixing the continuum level to the fits from Section 2.1. The line lists for the two observations differ substantially due to the fact that in obs. IV we do not find any line emission below 3.9 Å except for traces of an Fe K fluorescence line. In obs. III we detect all major H- and He-like Lyman  $\alpha$  lines plus a few weak H-like Lyman  $\beta$  lines from some elements. The fits to both spectra indicate no system-

atic or significant line shifts. Observation III appears to be slightly inconsistent with this assessment. The laboratory wavelengths tabulated in column 2 are taken from tables in the Atomdb web-guide. The difference in measured wavelength from the laboratory values for observation III distribute fairly well around a centroid shift of 0.0045 Å, which is well within the statistical and systematic uncertainties expected for this data set. In obs. IV there are fewer lines but they distribute well around the expected rest wavelengths.

The line shapes are resolved but require little broadening beyond the resolution of the HEG. Most Doppler broadening line velocities are less than 800 km s $^{-1}$ , except for Fe and some Mg lines. The 90% confidence limits indicate that the lines themselves are just barely resolved. There is no obvious correlation with wavelength scale except for the Fe region where the resolution is already over 1500 km s $^{-1}$ . The values for Mg stand out a bit. Specifically the fact that we could not resolve the Mg XI triplet indicates some higher velocity broadening. Since in both observations the lines are just barely resolved it is also not obvious if the trend to lower velocities in obs. IV is statistically relevant. Although the lines tend to be brighter, the fits suffer from lower contrast due to a higher continuum.

Another peculiarity between the line emission of obs. III and IV is the fact that we do not detect any emission lines with wavelengths shorter than Ar XVII in observation IV. Using the 1  $\sigma$  statistical uncertainty of the underlysing continuum we limit the line fluxes for the undetected line top below  $1.2 \times 10^{-6}$  ph s $^{-1}$  cm $^{-2}$ . While we do not detect Ar XVIII and Ca XIX in either absorption or emission, we detect Ca XX, Fe XXV, and Fe XXVI in absorption. Furthermore there is an unresolved line absorption complex longward of Fe XXV, likely due to lower transitions of Fe XX to XXII indicating the presence of both highly ionized and moderately ionized absorbers in the line of sight. We refer to these respectively as ‘hot’ and ‘warm’ components, although these designations do not reflect the fact that the dominant source of ionization is likely the continuum photons from the compact object rather than thermal electrons. The line positions of the hot absorption lines do not deviate significantly from the laboratory position. This is different to obs. I and II where they appeared blue-shifted, thereby producing P Cygni lines. A more detailed analysis of the absorbers is given below.

The Fe K region shows some peculiarities as well. In observation III the Fe XXV is clearly the dominant feature. It does show some excess flux longward of the forbidden line position, however with low statistical significance. Under the assumption that we are observing a photoionized plasma, then these could be trace contributions from inner shell transitions of Fe XIX – XXII ions (Kallman et al. 2004). If so, this would suggest the presence of a distribution of ionization parameters, extending to values  $\sim 10$  times less than the dominant component.

The main challenge for the photoionization model comes from the He-like lines, here Fe XXV, Ca XIX, Ar XVII, S XV and Si XIII and Mg XI, observed in obs III. In interpreting these lines we noted their dependence on gas

<sup>6</sup><http://heasarc.nasa.gov/docs/software/xstar/>

<sup>7</sup><http://heasarc.nasa.gov/docs/software/xspec/>

<sup>8</sup><http://space.mit.edu/CXC/ISIS/>

TABLE 2: THE CONTINUUM FIT RESULTS

Obsid	Model	$N_H$ [ $10^{22} \text{ cm}^{-2}$ ]	$N_H^{pc}$ [ $10^{22} \text{ cm}^{-2}$ ]	$f_{pc}$	$\Gamma_1$	$A_1$ [cts s $^{-1}$ Å $^{-1}$ ]	$\Gamma_2$ or kT $_{bb}$ [ $\text{keV}$ ]	$A_2$ [cts s $^{-1}$ Å $^{-1}$ ]	$\chi^2_\nu$
6148	P	$3.86^{+0.30}_{-0.29}$	—	—	$2.11^{+0.16}_{-0.15}$	$2.3^{+0.6}_{-0.5} \times 10^{-2}$	—	—	1.14
	PCBP	$2.86^{+0.07}_{-0.08}$	$4.46^{+0.45}_{-0.64}$	$0.95^{+0.02}_{-0.03}$	$1.40^{+0.03}_{-0.16}$	$6.8^{+0.2}_{-1.8} \times 10^{-3}$	$0.43^{+0.05}_{-0.03}$	$6.1^{+2.8}_{-0.6} \times 10^{-3}$	0.90
	PCPP	$1.88^{+0.06}_{-0.07}$	$1.84^{+0.08}_{-0.05}$	$0.92^{+0.04}_{-0.02}$	$1.87^{+0.03}_{-0.01}$	$1.6^{+0.6}_{-0.1} \times 10^{-2}$	$7.08^{+2.07}_{-1.07}$	$5.3^{+6.0}_{-0.3} \times 10^{-3}$	0.94
5478	PCPP	$5.92^{+0.05}_{-0.08}$	$12.67^{+0.09}_{-0.11}$	$0.95^{+0.01}_{-0.01}$	$1.67^{+0.00}_{-0.01}$	$0.26^{+0.00}_{-0.00}$	$5.99^{+0.26}_{-0.22}$	$8.4^{+0.6}_{-1.7} \times 10^{-2}$	0.84

P = Power law; PCBP = partially covered blackbody + power law ; PCPP = partially covered power law + power law

TABLE 3: X-RAY LINE PROPERTIES

Observation III					Observation IV		
ion	$\lambda_o$ Å	$\lambda_{III}$ Å	Flux $_{III}$ $10^{-4} \text{ ph s}^{-1} \text{ cm}^{-2}$	$v_{III}$ km s $^{-1}$	$\lambda_{IV}$ Å	Flux $_{IV}$ $10^{-4} \text{ ph s}^{-1} \text{ cm}^{-2}$	$v_{IV}$ km s $^{-1}$
Fe XXVI	1.780	1.783±0.002	0.97±0.20	1680±1490	1.776±0.001	−2.45±0.08	740±880
Fe XXVr	1.850	1.853±0.001	1.58±0.17	570±1130	1.848±0.002	−1.78±0.34	1090±850
Fe XXVi	1.859	1.860±0.002	0.80±0.15	1520±1200	—	—	—
Fe XXVf	1.868	1.870±0.001	1.07±0.15	570±1120	—	—	—
Ca XX L $\alpha$	3.021	3.023±0.002	0.26±0.06	210±450	3.019±0.001	−0.83±0.19	430±520
Ca XIXr	3.177	3.163±0.012	<0.07	<650	—	—	—
Ca XIXi	3.189	3.184±0.001	0.51±0.15	660±950	—	—	—
Ca XIXf	3.211	3.205±0.003	0.25±0.10	590±650	—	—	—
Ar XVIII L $\alpha$	3.734	3.738±0.005	0.40±0.13	590±990	—	—	—
S XVI L $\beta$	3.780	3.787±0.006	0.24±0.12	550±470	—	—	—
Ar XVIIr	3.949	3.939±0.004	<0.06	<610	3.932±0.005	<0.01	<660
Ar XVIIi	3.966	3.956±0.004	0.24±0.13	360±530	3.958±0.007	0.19±0.18	130±110
Ar XVIIf	3.994	3.995±0.003	0.45±0.15	600±520	3.998±0.005	0.34±0.19	600±490
S XV L $\beta$	4.310	4.310±0.006	0.28±0.15	610±220	—	—	—
S XVI L $\alpha$	4.730	4.737±0.001	2.12±0.24	540±320	4.734±0.003	1.82±0.40	420±390
S XVr	5.039	5.046±0.006	0.34±0.24	250±170	5.042±0.008	0.40±0.23	210±200
S XVi	5.067	5.056±0.007	0.40±0.30	780±440	5.070±0.015	0.31±0.27	210±200
S XVf	5.102	5.106±0.005	0.44±0.15	720±910	5.103±0.006	0.60±0.26	270±260
Si XIV L $\beta$	5.217	5.222±0.005	0.55±0.25	390±510	5.225±0.007	0.53±0.30	300±330
Si XIV L $\alpha$	6.183	6.192±0.001	1.54±0.18	550±110	6.185±0.002	3.43±0.47	490±230
Si XIIIr	6.650	6.662±0.005	0.24±0.11	280±310	6.643±0.007	0.69±0.33	390±480
Si XIIIi	6.669	6.690	<0.11	<310	6.705±0.010	0.21±0.25	160±580
Si XIIIf	6.740	6.746±0.005	0.30±0.09	800±410	6.741±0.003	1.12±0.34	290±290
Mg XII L $\beta$	7.106	7.104±0.012	0.36±0.13	1450±1100	7.109±0.007	1.07±0.40	690±530
Mg XII L $\alpha$	8.422	8.432±0.005	1.40±0.33	670±200	8.422±0.007	4.65±1.43	690±370
Mg XI(r,i,f)	9.230	9.219±0.084	2.31±1.01	3940±680	—	—	—

density and excitation mechanism (Bautista & Kallman 2000; Porquet & Dubau 2000): each line complex consists of three components, denoted r, i, f, ordered in increasing wavelength. At densities below the critical density we expect  $R=f/i \geq 1$ , and conversely. Critical densities depend on the nuclear charge,  $Z$ , and range from  $\sim 10^6 \text{ cm}^{-3}$  for C to  $\sim 10^{17} \text{ cm}^{-3}$  for Fe. Gas that is photoionized is expected to emit these lines primarily by recombination cascade, and will have  $G=(f+i)/r \geq 1$ . Gas which is excited by electron collisions, or in which resonantly scattered emission is important, will have  $G \leq 1$ . The He-like complexes in obs. III all provide us with constraints on the excitation mechanism and gas density, although taken together they provide conflicting indications of these quantities. The Fe XXV feature peaks near  $1.86 \text{ \AA}$ , which is the rest energy of the intercombination line, but it extends beyond  $1.87 \text{ \AA}$ , the energy of the forbidden line, and there is little emission at  $1.85 \text{ \AA}$ , the energy of the resonance line. The Ca XIX line behaves similarly. We only measure an upper limit to the resonance line, but find strong intercombination and weak forbidden lines. However, there is excess emission at wavelengths greater than the laboratory wavelength of the forbidden line, which cannot be adequately fitted by the XSTAR model. Ar XVII is an intermediate case in which the fit accepts both a resonance line and a forbidden line. S XV is an intermediate case as well, though its line components appear less significant. Si XIII is a clearer case, and we have data from both observations. Figure 4 shows the spectrum in both cases, in which the resonance and forbidden lines are clearly detected and the intercombination lines are upper limits. This suggests a density below the critical density for the  $2s^3P - 2s^3S$  transition, which is  $5 \times 10^{14} \text{ cm}^{-3}$  for Si. The He-like line ratios from the heavier elements suggest that if there is a single plasma density it is likely near that limit. Although we cannot resolve Mg XI in obs. III, the line clearly peaks at the location of the intercombination line indicating an R ratio well below 1 and thus densities significantly above  $10^{13} \text{ cm}^{-3}$  (see also the discussion in Sect. 4.1).

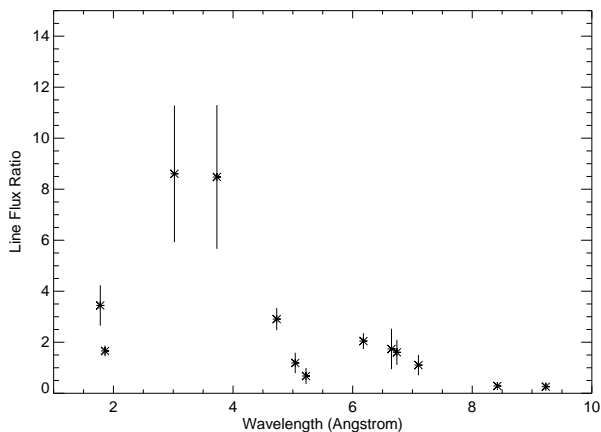


FIG. 3.— Flux ratios  $f_{III}/f_{III}$  for lines measured in obs. III and II (values taken from SBII).

The fluxes of the emission lines are shown in Table 3. The lines in obs. IV appear bright with fluxes between  $2 \times 10^{-5}$  and  $3.4 \times 10^{-4} \text{ ph cm}^{-2} \text{ s}^{-1}$ , in obs. III ranging from  $1.5 \times 10^{-5} \text{ ph cm}^{-2} \text{ s}^{-1}$  to  $2.1 \times 10^{-5} \text{ ph cm}^{-2} \text{ s}^{-1}$ .

<sup>9</sup><http://heasarc.gsfc.nasa.gov/docs/software/xstar/xstar.html>

The line fluxes between the two observations are not substantially different from each other, most pre-zero phase fluxes seem slightly lower. This is different from what we observed during the high flux states (SBII) where the line fluxes differed substantially. The flux difference between pre- and post-zero phase then also was an order of magnitude larger than what we observe now. Another issue arises when we compare the pre-zero phase lines between obs. II and III (see Figure 3). The reason we use observation II is because here we expect the least perturbing effects of pileup on the lines. The source flux in obs. II was determined to be  $4.8 \times 10^{-9} \text{ erg cm}^{-2} \text{ s}^{-1}$  which leads to a continuum flux ratio of about 150. In case that we observe a similar photoionization regime, we would expect that the line ratios are very similar to this flux ratio. The ratios in Figure 3 appear much smaller than this expectation. Some of this effect is certainly caused by pileup in obs. II which likely causes the slope from large to small wavelengths. Even with some of the line fluxes reduced by pileup effects, the line ratios fall still well short of the expectation from the continuum ratios, which besides the effects of the now reduced source luminosity we attribute to additional absorber activity as well as a more dramatic change in ionization balance.

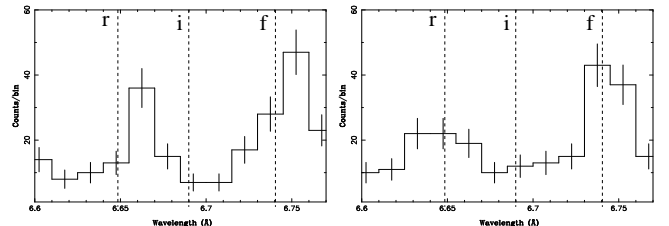


FIG. 4.— The Si XIII triplet from Obs. III (left) and IV (right). In both triplets the forbidden line is the strongest and the intercombination line is weak. The slight redshift for obs. III is within the systematic uncertainty of the wavelength scale.

### 3.2. Photoionization Fits with XSTAR

The spectral analysis based on Gaussian fits indicates complex ionization structures. First we investigate photoionization in observation III. For the XSTAR fits we use the PHOTEMIS analytic model in XSPEC, which is available from the XSTAR website.<sup>9</sup> This model generates a line spectrum characterized by element abundances, velocity turbulence, ionization parameter and normalization. Density is not a free parameter in the fits, but it can be varied by importing XSTAR model runs calculated at various density values. Temperature is also not a free parameter in these fits, since it is calculated self-consistently by XSTAR under the assumption that heating due to photoionization is balanced by the radiative cooling of the gas. The determination of the ionization parameter is of the most interest in this analysis.

The model spectrum produces all the lines listed in Table 3 and reproduced the listed fluxes within the quoted errors for over 75% of the lines. The lines are slightly broadened (see above) which was reflected in a turbulence velocity parameter of  $300 \text{ km s}^{-1}$ . The temperature of the photoionized plasma is largely set by the detection of radiative recombination continua. Since there are no significant detections of these, the temperature of the plasma



TABLE 4: THE FIT RESULTS USING THE PHOTOIONIZATION (PH) AND WARMABSORBER (WA) MODEL IN XSTAR

Obsid	Model	$\log N_H^{cold}$ [cm <sup>-2</sup> ]	$\log N_H^{warm}$ [cm <sup>-2</sup> ]	$\xi$ [ergs cm s <sup>-1</sup> ]	$\Gamma$	z	$f_x^a$	$L_x^b$ [10 <sup>36</sup> erg s <sup>-1</sup> ]
6148	PH	22.9 <sup>+0.0</sup> <sub>-0.0</sub>	—	3.0	1.58 <sup>+0.00</sup> <sub>-0.00</sub>	0.001	1.219	0.79
5478	WA (quies.)	22.3 <sup>+0.1</sup> <sub>-0.1</sub>	23.9 <sup>+0.1</sup> <sub>-0.0</sub>	1.6 <sup>+0.4</sup> <sub>-0.2</sub>	0.38 <sup>+0.29</sup> <sub>-0.19</sub>	-0.0077 <sup>+0.0028</sup> <sub>-0.0047</sub>	1.51	1.4
5478	WA (flar.)	23.4 <sup>+2.4</sup> <sub>-0.7</sub>	22.8 <sup>+0.1</sup> <sub>-0.1</sub>	2.7 <sup>+0.1</sup> <sub>-0.2</sub>	2.62 <sup>+0.12</sup> <sub>-0.12</sub>	-0.0019 <sup>+0.0019</sup> <sub>-0.0021</sub>	8.31	9.9

a)  $\times 10^{-10}$  erg cm<sup>-2</sup> s<sup>-1</sup> between 2 – 10 keV

b) for a distance of 6 kpc

must be greater than 10<sup>6</sup> K which blends these features into the continuum; the temperatures of the XSTAR models at the best-fit ionization parameter are consistent with this constraint. The density of the plasma is determined by the He-like triplets. As indicated in Sect. 3.1, the triplets provide conflicting trends. The fit allows a lower density solution as suggested predominately by the Si XIII triplet with  $\sim 10^{14}$  cm<sup>-3</sup>, which is only in conflict with the density constraints from Ca XIX and Fe XXV, which seem to suggest  $> 10^{15}$  cm<sup>-3</sup>. An ionization parameter ( $\xi = L_x/(nr^2)$ ) of  $\log \xi = 3.0 \pm 0.1$  gives the best result and provides a cold column of  $7.9 \pm 0.1 \times 10^{22}$  cm<sup>-2</sup>, a power law index of  $\Gamma = 1.58 \pm 0.1$ , and a total X-ray flux of  $1.22 \times 10^{-10}$  erg cm<sup>-2</sup> s<sup>-1</sup>. The fitted flux and power law index are consistent with our continuum analysis. XSTAR also allows some constraint on abundance and although some slightly higher abundances are seen for Si and Ca, the fit clearly required significantly enhanced Fe.

### 3.3. Line Emissivities and Predictions

It is straightforward to explore the implications of our measurements of emission line fluxes for models for the accretion flow in Cir X-1. For example, from the Gaussian fit to the lines we find a net flux of approximately  $7.9 \times 10^{12}$  erg cm<sup>-2</sup> s<sup>-1</sup> in the lines making up the Fe XXV K complex. At a distance of 6 kpc this corresponds to a line luminosity of  $3.2 \times 10^{34}$  erg s<sup>-1</sup>. If this were emitted by recombination in a region with uniform conditions, the luminosity would be:

$$L_{line} = n^2 V \alpha_{2p} \varepsilon_{line} x_{FeXXVI} y_{fe} \quad (1)$$

where  $n^2 V$  is the emission measure,  $\alpha_{2p}$  is the effective recombination rate into the 2p levels of Fe XXV,  $\varepsilon_{line}$  is the line energy  $x_{FeXXVI}$  is the ion fraction of Fe XXVI and  $y_{fe}$  is the iron elemental abundance. From XSTAR models we have  $\alpha_{2p} x_{FeXXVI} = 1.95 \times 10^{-12}$  cm<sup>3</sup> s<sup>-1</sup>. Combined with the measured line luminosity, we find that the emission measure at  $\log(\xi) = 3$  must therefore be  $n^2 V = 4.9 \times 10^{58}$  cm<sup>-3</sup>.

This quantity can be compared with what is expected from an X-ray heated accretion disk coronae (ADC) in low mass X-ray binaries. Simple estimates for the emission measure distribution from an ADC are complicated, owing to the fact that the coronal temperature, density and ionization are coupled by the constraints of hydrostatic equilibrium, thermal balance, and the radiative transfer of photons into the corona. Calculations for the ADC structure including these effects have been published by

London (1982); Begelman et al. (1983); Kallman & White (1989); Ostriker et al. (1991); Ko & Kallman (1994); Rózańska et al. (2002); Jimenez-Garate et al. (2002), and many others. A simple estimate for the distribution of emission measure with ionization parameter

$$\frac{dEM}{d\xi} = \int n^2 2\pi R dR \frac{dz}{d\xi} \quad (2)$$

can be obtained using an isothermal approximation to the disk vertical structure:  $n(z) = n_0 \exp(-(z/z_s)^2)$ , where the scale height is  $z_s = \sqrt{(kTR^3/(GMm_H))}$ . Then:

$$\frac{dEM}{d\xi} \simeq \xi^3 \left( \frac{kT}{GMm_H R_i^3} \right)^{1/2} L^2 = 2.5 \times 10^{65} \xi^{-3} L_{38}^2 R_{i7}^{-3/2} T_4^{1/2} \quad (3)$$

where  $L_{38}$  is the source luminosity in units of 10<sup>38</sup> erg/s,  $R_{i7}$  is the disk inner radius in units of 10<sup>7</sup> cm and  $T_4$  is the corona temperature in units of 10<sup>4</sup> K.

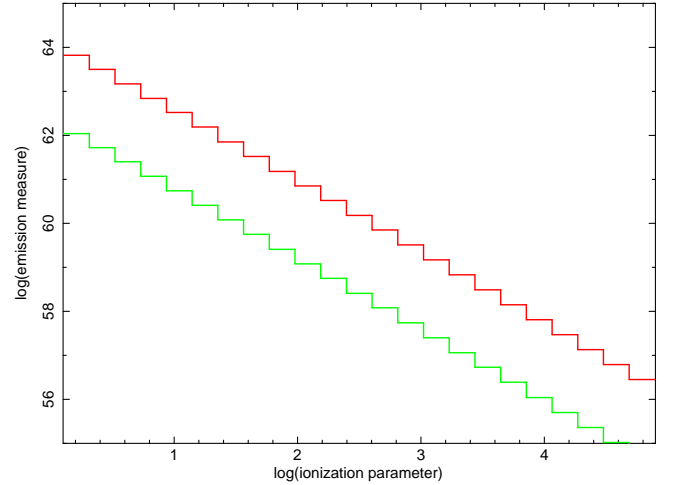


FIG. 5.— Calculation of emission measure in dependence of ionization parameter for a static corona for two different luminosities,  $L = 10^{38}$  erg s<sup>-1</sup> (red) and  $L = 10^{37}$  erg s<sup>-1</sup> (green).

This result is quite accurate when compared with the results of numerical solutions for a single-stream treatment of the transfer of the X-rays, and for a disk around a 1  $M_\odot$  compact object extending from 10<sup>7</sup> to 10<sup>11</sup> cm. Figure 5 shows such a calculation, for  $L_{38} = 1$  (red curve) and  $L_{38} = 0.1$  (green curve). This shows that at  $\log(\xi) = 3$ , an emission measure that we infer from the observations can only be produced by an ADC if the source luminosity is well above 10<sup>37</sup> erg/s. Although this estimate of emission



measure is idealized, and assumes a static corona above a thin disk, it is clear that the continuum luminosity needed to produce the line emission we observed exceeds the luminosity we infer from continuum fits by a factor almost two orders of magnitude. One possible explanation for this is that the true luminosity intrinsic to the source is much greater than what we observe, and that the apparent low state is a consequence of obscuration or collimation of the radiation into a direction away from our line of sight.

#### 3.4. The warm absorber in observation IV

Figure 6 clearly indicates that the hard spectrum in obs. IV has not only changed in its continuum properties, but also exhibits complex absorber activity. Encouraged by the similarity of the line spectra above about 4 Å in obs. III and IV we use the results from Sect. 3.2 in the modeling of the post-zero phase spectra. We adopt two XSTAR components to model the spectrum in obs. IV, the warm absorber model (WARMABS) plus the photoemission model (PHOTEMIS) determined from observation III. The data quality is not sufficient to constrain all the parameters of both components unambiguously, so in order to reduce the number of free parameters we fix the photoemission component to the one fitted in observation III. This choice also makes sense under the presumption that dips are generated by blocking the central X-ray source and thus exposing the accretion disk coronal spectrum as observed in, for example, dipping sources like EXO 0748-676 (Jimenez-Garate et al. 2003). The foremost photoionization parameters we freeze from the above analysis are the ionization parameter for the photoemission, the normalization and the turbulence velocity parameter. In a second step we recognize that the obs. IV shows significantly more variability than obs. III. We then separated the quiescent segments in the light curve of obs. IV (see Figure 1) and the flaring segments.

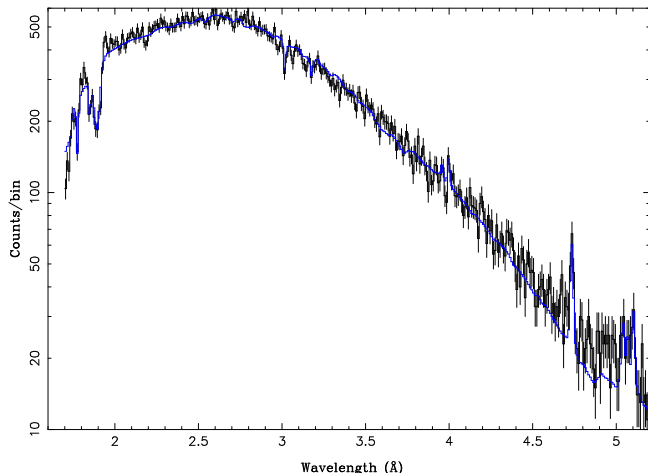


FIG. 6.— The total spectrum below about 5 Å from obs. IV showing photoemission of the soft side but complex photoabsorption on the hard side.

In the following we denominate the two levels accordingly as “quiescent” and “flaring” states. Table 4 shows the results of the XSTAR fits to the quiescent and flaring state. The model fits well to both states and produces significantly different results. During the quiescent state the warm absorber model results in a low ionization parameter

of  $\log \xi = 1.6 \pm 0.3$ . The absorption feature at Fe K then corresponds to absorption from Fe XVI – XVIII. The cold column seems reduced with respect to the one observed in obs. III, but a warm column of  $7.9 \times 10^{23} \text{ cm}^{-2}$  appears. In the flaring state the cold column is reduced as well with a lower warm column of  $6.3 \times 10^{22} \text{ cm}^{-2}$  but a high ionization parameter of  $\log \xi = 2.7 \pm 0.2$ . The absorber near Fe K has its strongest contributions now from Fe XXI-XXIII. In order to obtain the best fit a blueshift of approximately 600 km s<sup>-1</sup> is adopted. However, this value yields a fit which is only marginally improved ( $\Delta\chi^2 \simeq 3$ ) compared with no blueshift. Similarly, tests of the fits to the obs. IV data with and without the emission component show marginal improvement ( $\Delta\chi^2 = 8$  for the flaring state and  $\Delta\chi^2 = 6$  for the quiescent state). Table 4 allows lists the total luminosities for the two WA cases.

Figure 7 shows the dependence of the depths of observed absorption lines on ionization parameter for the flaring state. The fiducial optical depth is chosen arbitrarily, i.e. the column density of the absorber. Plotted is the log of the ratio of the optical depth produced by an XSTAR model with total column density  $10^{22} \text{ cm}^{-2}$  and solar abundances (Grevesse & Sauval 1999) to the observed depths. Most curves intersect near  $\log \xi \sim 2.7$ .

These were determined using a simple Gaussian fit to the lines, and the plotted error bars reflect the statistical error associated with these fits. This shows the range of  $\xi$  which is approximately consistent with the observations, and also illustrates the nature of the constraints: the Fe XXVI line constrains ionization parameter on the low side, and the Si and S lines constrain the ionization parameter on the high side.

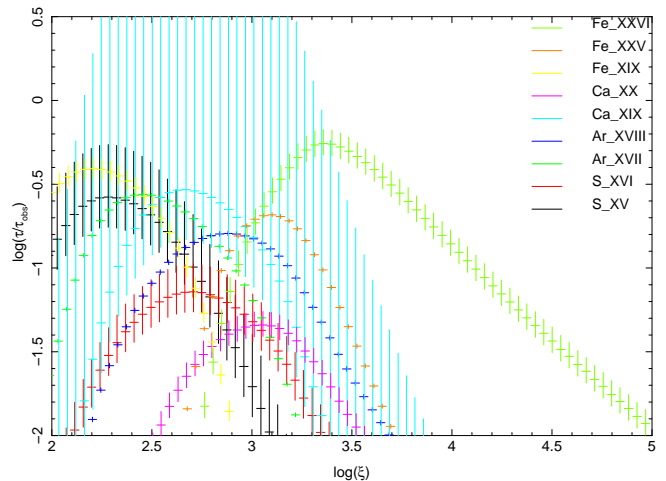


FIG. 7.— The dependence of the depths of observed absorption lines on ionization parameter for the XSTAR fits in the flaring state.

#### 4. DISCUSSION

The at times ultraluminous X-ray source Circinus X-1 has been observed by nearly all X-ray missions over the last 30 years, and it seems that the source continues to provide a plethora of new features in its X-ray emission. The light curves, as expected from the monitoring with the ASM, show much less activity before but also after zero orbital phase. This confirms that the source has moved into a novel physical state. In fact, we suspect that Circinus X-1 was still in transition because since January 2007

until the submission of this paper the X-ray flux dropped under the detection limit of the ASM. Whether the source is in the process of turning off or reaching a defined minimum is unknown. We suspect the latter if we follow the 30 yr light curve compiled by Parkinson et al. (2003), though this light curve does not provide fully continuous coverage during its previous low-flux periods that lasted between 1971 and 1986. The analysis in this paper aims to identify the physical state of the X-ray emitting plasma and draw conclusions about the source's condition while it transits towards lower fluxes. We also put these findings into context with the sources' previous high-flux behavior.

#### 4.1. Some General Remarks

There are still many outstanding questions concerning the detailed nature of the system. Besides its identification as an accreting neutron star (Tennant et al. 1986), there is circumstantial evidence that Cir X-1 could be a Z-type LMXB (Schulz, Hasinger & Trümper 1989; Hasinger & van der Klis 1989) based on its spectral variation pattern in the color-color diagram (e.g., Shirey et al. 1999; Ding, Qu & Li 2006). However, given recent findings, it has to be a quite peculiar one for several reasons. Its long-term light curve fits more the description of an X-ray transient with excursions from 1 – 2 Crab to less than a mCrab (Parkinson et al. 2003). Our observations, as well as recent *SWIFT* and *RXTE* observations (Jonker et al. 2007a), show that Cir X-1 has gone from an all-time high during the 1990s into an extended low-flux state where the source dropped to a flux of  $3 \times 10^{-11}$  erg s $^{-1}$  corresponding to a luminosity that is below  $10^{35}$  erg s $^{-1}$ . LMXBs that low in luminosity are rare and the detection of an LMXB close to the Galactic Center with a luminosity of only  $4 \times 10^{34}$  erg s $^{-1}$  but high-luminosity outbursts (Muno et al. 2005) may indicate the existence of a peculiar class of LMXB transients. Conventional Z-source do not behave that way, and even atoll sources are brighter in their hard states. A most compelling indication that Cir X-1 is indeed a neutron star is a recent detection of twin kHz quasiperiodic oscillations (QPOs) during the high-flux state (Boutloukos et al. 2006), which seem in good agreement with Z-sources, but not with black-hole binaries. Furthermore, the discussion about the companion has received attention again more recently as Jonker et al. (2007b) produced some evidence that the companion star of Cir X-1 is of intermediate mass and of types B5 to A0. This is unusual for a Z-source, as the ones known all have low-mass companions.

Jonker et al. (2007b) constrain the companion mass to  $< 10 M_{\odot}$  and the angle of inclination to be  $> 14^{\circ}$ . The angle of inclination has been under dispute since evidence for ultrarelativistic radio jets was presented (Fender et al. 2004a). An angle of  $< 5^{\circ}$  became a natural choice under the assumption that the energy injection happened during the last zero-phase outburst and that there is no bending. However, there is no evidence for this correlation. Neither recent claims of soft excesses (Iaria et al. 2005) nor unabsorbed soft components (Ding, Qu & Li 2006) can be substantiated in our high-resolution spectra during the low-flux state here and in the high-flux state years ago (see also SBII, Galloway et al. 2007), and any claims referring to the angle of inclination likely do not apply.

In Ding, Qu & Li (2006) it was suggested that this excess could come from the accretion hot spot and its large emission volume would then rule out a large inclination. However the spectral analysis presented seems clearly tainted by an unrealistically high Fe K line flux. Besides the fact that the continuum above the Fe K edge cannot physically produce such a line strength, we resolved Fe K lines in the high state and found them to be two orders of magnitude lower in strength (SBII). This leaves us with the unfortunate reality that we are still quite uncertain about the angle of inclination.

If the result that the companion is of intermediate mass holds up, our analysis can very much rule out a possible later B-type stellar wind as the region of origin for the X-ray lines. Later type B-stars with surface temperatures above  $10^4$  K can still maintain substantial winds. The size of the system is about  $5 \times 10^{12}$  cm (Tauris et al. 1999) which for the measured ionization parameter results in densities of the order of  $4 \times 10^6$  cm $^{-3}$ , which even for a late B-types seems quite low. The He-triplets suggest much higher densities than that which places the ionization region much closer to the X-ray source. We also measure significantly enhanced Fe in the photoemission, which is quite hard to argue for in an early type stellar wind.

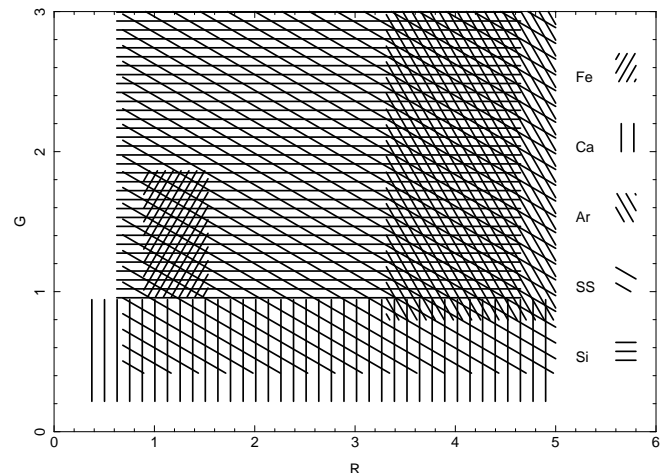


FIG. 8.— The range of R and G ratios for the He-like line emission in Obs. III.

Before we discuss emission regions in more detail, we have to address our difficulties determining a plasma density from the He-like triplets. Though we are somewhat plagued by bad statistics and some uncertain systematic effects, we still expected a more consistent picture. To date our ability to diagnose the high-density regime has always been limited by the unavailability of data and these observations are a rare exception. The Mg IX triplet indicates an R-ratio  $\ll 1$  which puts a lower limit on the density of  $10^{13}$  cm $^{-3}$ . Figure 8 shows a cartoon relating the R-ratios with the corresponding G-ratios. High-density regimes are a consistent solution for all triplets but Ar XVII, which is however statistically weak. Ca XIX, on the other hand, though it would be consistent with high density, does not fit into the recombining regime and appears more collisional. Fe XXV provides the tightest solution for higher density, but is also close to a collisional solution. Though all in all a density of  $\sim 5 \times 10^{14}$  cm $^{-3}$  in a recombining gas seems most plausible, we want to caution that there

are remaining inconsistencies, which, given the turbulent nature of the system, could indicate time-dependent aspects and a situation where our equilibrium assumption may not be entirely valid.

#### 4.2. The Photoionized Disk Corona

Quite evidently, the P Cygni lines found during the early *Chandra* observing cycles (BSI, SBII) are not present in the new spectra. So far these line profiles still stand unique for this class of objects. The last time we observed these P Cygni lines was during a short observation of Cir X-1 at phase 0.25 during the year 2001 (Galloway et al. 2007). The interpretation at the time was that the profiles are a result of a preferentially equatorial wind driven by the central source. In observation III, the overall source flux was reduced by over two orders of magnitude with respect to the 2000 observations and one of the questions to answer is if this is a true reduction in source luminosity or an effect of increased circumstellar/circumdisk absorber activity. Our direct comparison of the ratio of the line fluxes with the ratio of the continuum fluxes suggests that absorption is playing an important role, even though that comparison is tainted by the pileup problems during the high-state observations. On the other hand, photoionized plasmas are complex and we have to look at the change in ionization balance between the high and now low flux phases represented by the ionization parameters. Although we were not able to directly measure  $\xi$  in obs. I and II we could infer parameters well in excess of  $10^4$  using calculations from Kallman & Bautista (2001). Our fits to obs. III resulted in an ionization parameter of  $10^3$ , which is an order of magnitude lower. Thus significant dimming of the X-ray flux thereby changing the ionization balance provides a solution that would not require significant additional absorption. Thus the comparison of line and continuum fluxes and the comparison of ionization balances have quite different implications. In that sense the observed X-ray emission may not provide a full account of the true energy balance near the central source and we have to acknowledge the fact that there has been no significant long-term increase in the observed cold column between the high and the low flux states for the years 2000 and 2005, respectively.

At this point it seems necessary to invoke some model assumptions about accretion dynamics. In order to test the assumption that the photoemission region could be the accretion disk we compare results from our XSTAR fits of obs. III to some simple model predictions. As a basis for these tests we use some of the models described by Jimenez-Garate et al. (2002), who modeled an accretion-disk atmosphere and corona photoionized by a central X-ray continuum source and also discuss feedback mechanisms between disk structure and the central illumination. In this model we assume an optically thick standard disk (Shakura & Sunyaev 1973) with a heated atmosphere, which is separated from the disk by a  $\tau = 1$  surface, sometimes called photosphere. The atmosphere is strongly heated resulting in evaporation into a hot corona and eventually leads to outflows. The plasma above the photosphere is heated up to  $10^7$  K and cools through atomic line emission. The most important parameter to investigate the state of the plasma is the ionization parameter  $\xi$ .

In order to determine the source luminosity  $L_x$  we assume a source distance of 6 kpc. The distance is not well known but it is widely agreed that the source is not closer than this. The claim by Iaria et al. (2005) of 4.1 kpc has been recently dismissed by Jonker et al. (2007b) who actually favor a distance of  $\sim 8$  kpc. For the density  $n$  we have some indication from the He-like triplets, but plausibility arguments are still needed.

In the inner disk under the idealistic assumption that viscous heating and radiative heating from an illuminating source is locally expressed by a blackbody, radiative heating should dominate over viscous heating at radii larger than  $2.3 \times 10^8$  cm (Vrtilek et al. 1990). With a luminosity of  $8 \times 10^{35}$  erg s $^{-1}$  we expect an upper limit to the density of  $\sim 10^{16}$  cm $^{-3}$ . The strength of the forbidden line in the Si XIII argues against such a high density and if we employ our projection of  $\sim 5 \times 10^{14}$  cm $^{-3}$ , we place the emission region at a radius of  $\sim 10^9$  cm. During the high flux in the year 2000 we projected a launching radius  $> 10^{10}$  cm and densities  $> 5 \times 10^{13}$  cm $^{-3}$ , which given the higher source luminosity seems consistent.

As shown in Sect. 3.3 luminosities which can heat an ADC have been observed during the high-state of the source. The luminosities inferred during the observations reported here are significantly lower. This suggests that either there are problems with the static corona approximation or that there are unobserved photons or other heating mechanisms responsible for the coronal excitation. We do not see any obvious signs for winds in our data like in the year 2000 observations, however there still seems to be jet activity in the radio (P. Jonker, priv. comm.). On the other hand, the problem of insufficient heating power for ADCs as derived from X-rays does not seem to be unique to Cir X-1. The emission measures determined in classical ADC sources such as 4U 1822-37 (Cottam et al. 2001), EXO 0748-676 (Jimenez-Garate et al. 2003), 2S 0921-63 (Kallman et al. 2003) and HerX-1 (Jimenez-Garate et al. 2005) are greater than the ADC model can produce based on the observed luminosity. In the case of Her X-1 it has been suggested that the energy range is indeed much dominated by absorption (Kuster et al. 2005; Ji et al. 2007) and the luminosity in its low-state may be higher than observed. If this is the case, then the ionization balance we observe in the low-state of Cir X-1 should also be largely dominated by obscuration rather than a true reduction in source luminosity and as such would suggest a genuine analogy to a Seyfert II.

All the sources mentioned above have high angles of inclination ( $85^\circ \lesssim i \lesssim 90^\circ$ ) which given the strong similarity of the low-state spectral properties in Cir X-1 is a confirmation of the previous X-ray projection of a higher angle of inclination. However, there are two distinct differences between these sources and Cir X-1. One is the fact that we have a history of the source of once being very luminous exhibiting powerful winds, the other one is its jet activity which even in the low-flux state seems to be prevailing. Generally almost two orders of magnitude in luminosity are not easily hidden by absorption and the relative constancy of  $N_H$  in Cir X-1 over the years is difficult to reconcile with a simple obscuration paradigm. The fact that the luminosity changed from a level that seemed

sufficient to sustain a static corona in the high-state to a gross deficiency in the low-state without much change in absorption properties between obs. II and III also leads to questioning whether the assumption that the X-ray luminosity is the dominating heating component and/or the assumption of a simple static corona is correct.

Jet and wind activity indicates that the disk in Cir X-1 may be cooling more efficiently than predicted from standard models and additional energy is transferred into the corona or the jet base. The connection of compact ADCs and the base of jets has been made recently in a study by Markoff, Nowak & Wilms (2005). Though it is well beyond the scope of this paper to go into details, we have to address the possibility that other mechanisms than X-ray illumination can heat the corona. Recent studies clearly emphasize the role of magnetic activity.

Relativistic jets are a fundamental aspect of accretion on to black holes (Fender, Belloni & Gallo 2004b) and much emphasis in recent years has been devoted to investigate connections between compact ADCs and jet activity Merloni & Fabian (2002); Markoff, Nowak & Wilms (2005); Krolik, Hawley & Hirose (2007). The formation of jets may arise from radiation pressure (Lynden-Bell 1978; Begelman & Rees 1984) or magnetic fields (Blandford & Znajek 1977) and since we deal with X-ray luminosities well below  $L_{\text{edd}}$  we may argue for the latter as the underlying scenario. Viscous turbulence in the accretion flow is now understood to be due to the magnetorotational instability (MRI, Balbus & Hawley 1998) and it may as well also be the source for a magnetically dominated corona (Merloni & Nayakshin 2006). Observational evidence for MRI effects in GRO J1650-55 has recently been presented by Miller et al. (2006c). The low-flux observations presented in this paper fit most criteria that qualifies the low-flux state as some form of low/hard state as seen in accretion black hole binaries (see Fender, Belloni & Gallo 2004b; Miller et al. 2006b and references therein).

#### 4.3. The Absorber Region

The fact that there is a significant warm absorber in the post-zero phase spectra is obvious through the broad absorption feature around 1.9 Å. In hot gases, where the electrons are generally stripped out of their atomic bond, absorbing fractions are usually generated by the formation of a significant number of He-like and H-like ion states. Such absorption has been observed in many accreting X-ray binaries, some show ionization fractions only for iron, some throughout the X-ray band down to oxygen. Circinus X-1 in this respect was pioneering as the *Chandra* first observations at the end of the high flux period showed blueshifted absorption lines for most detectable H- and He-like ions species. On top of this phenomenon we could show in SBII that the equivalent widths of the hot absorption is tightly linked to the slope variation of the underlying continuum.

The changes we see in the warm absorber are a bit more subtle but point in a similar direction. We now observe an entirely different ionization regime and the atomic physics is more complex due to the fact that in this absorber we do not have simple He-like and H-like ions. Atomic data covering this ion regime has not been available until recently

when Kallman et al. (2004) updated the XSTAR database specifically in the Fe K band. Model simulations indicated that under very specific circumstances 1s-np autoionizing transitions become dominant. The results are Fe XVII - XIX absorption features near 1.9 Å and the Fe K edge. The appearance of this edge becomes increasingly diluted as the ionization parameter increases. The model regime then predicts warm columns of  $10^{23.5} \text{ cm}^{-2}$  and ionization parameters well below 100.

The unique ionization regime that produces the observed absorption makes the interpretation of the absorption relatively simple and straight forward. An optically thick cool and distant plasma is illuminated by a moderate source luminosity producing low-ionization ions. What makes the situation more complex is the fact that we observe at least four absorber regimes: a cold absorber, a “luke-warm” absorber during quiescence, a warm absorber during flares, and last but not least a hot absorber during both phases.

**The cold absorber:** In all our observations we detect cold photoelectric absorption at levels significantly above the expected line-of sight-columns. In obs. III we observe about  $8 \times 10^{22} \text{ cm}^{-2}$ , in obs. IV it is slightly lower in quiescence. Compared with obs. I and II from the high flux state of the year 2000 these numbers are not so much different. If we compare our results from the partial coverage fits with the ones in SBII, but also with the ones from the ASCA spectra a few years earlier (Brandt et al. 1996) then cold absorption remains at a rather steady level for long time periods. The cold absorber should be devoid of significant ionization fractions above Fe X in the X-ray band which limits the ionization parameter to below 1 and puts the material at a distance consistent with the outer accretion disk, i.e. beyond  $10^{11} \text{ cm}$ . The amount of cold material so far seems to be fairly invariable. Not only is it rather constant at zero orbital phases, but the edge optical depth remained constant throughout other binary orbit phases (Galloway et al. 2007) indicating similar amounts of cold material at all times.

**The luke-warm absorber:** The fits at quiescence shows an enormous warm column of  $8 \times 10^{23} \text{ cm}^{-2}$ . This warm absorber shows up in addition to the cold column. The slight reduction in cold column can be easily seen at the expense of a slightly increased source luminosity. It is evident, however, that this large amount of material has not been in the line of sight during the pre-zero phase obs. III as otherwise it could have only been exposed through a luminosity decrease, which would have rendered the warm absorber to a cold one. There are two possible time lines of how the matter got there. Either the material crept up over the time period between the observations, or we see newly accreted matter just after the incoming neutron star-disk system re-connected with the companion. Given the invariability of the cold column over several observing periods and that a sudden increase in mass accretion at zero orbital phase is expected (Tauris et al. 1999) we consider the latter possibility as more likely. During the high flux phase we did not see this effect as there the material was almost completely ionized at all times. This material, on the other hand, is then likely related to the material causing heavy dipping activity during that flux period Brandt et al. (1996); Shirey et al. (1999).

**The warm absorber:** The reason why we separate the absorber in quiescence and during flaring periods is that due to the large increase in source luminosity the absorber also experiences a change in ionization balance which also create higher transition Fe ions. The amount of warm column is now only  $6.3 \times 10^{22} \text{ cm}^{-2}$  which is an order of magnitude lower than during quiescence. There may two causes we can consider for the reduction. First, the source is actually accreting and thus mass moves towards the central source. This flow is usually subsonic (Frank, King & Raine 1992) and matter moves out of the ionization regime on timescales much larger than the entire observing time. The light curves in Figure 1 feature flaring periods of only a few hours. More likely is a feedback effect from direct accretion. Accreted matter is converted into X-rays further heating the absorber. The increase in cold absorption during flaring may simply reflect the change in ionization state of accreted matter.

**The hot absorber:** The fact that we also detect H- and He-like absorbers in the spectra also indicates the existence of a hot absorption component which reveals itself in resonance absorption of Ca XX, Fe XXV, and XXVI. The positions of the lines are not blue-shifted as observed during the high flux phases indicating that this absorber is not a wind but a stationary component. The hot absorber is likely part of the warm absorber reflecting the upper end of the spectrum of ionization fractions.

The light curve of obs. IV shows that final accretion has two components. In quiescence matter is supplied at a fairly steady level. During flares accretion also comes in chunks of different sizes which is reflected by the very short flare onsets and types. Average rise times are less than a few minutes. Large flares are accompanied by a staccato of many subflares indicating rather turbulent ac-

cretion. Most remarkable is the correlated change of absorber column and ionization fraction with the luminosity. Although our data only allow us to analyze the integrated spectra of quiescent and flaring intervals, this analysis indicates that all the absorbers are connected and the source behaviour may be explained by varying illumination levels of the absorbers combined with varying obscuration levels of the central source.

There are many places in the system where this can happen. Based on the observed ionization fractions, most of the material should be at larger radii from the source than the photo-emission regions. This is likely also true for the hot absorber, which can be seen by the fact that during flares, the flux of most emission lines are reduced. The increase in source luminosity cannot remove these ionization fractions which should survive at even much higher luminosities as we have observed during obs. II (SBII). Although we cannot rule out other more exotic options a most logical place for the absorbers is the mid-and outer disk atmosphere/corona which in turbulent systems such as Cir X-1 can puff up to fairly large scale heights. Even in this case, though, we would limit inclination to higher than  $60^\circ$  (see also Jimenez-Garate et al. (2002)) as we proposed perviously (BSI, SBII, Schulz et al. 2006). The variable absorber activity we observe together with the complex play of warm column and luminosity (see Table 4) again underlines the importance of obscuration effects and the Seyfert II analogy.

We thank all the members of the *Chandra* team for their enormous efforts. We gratefully acknowledge the financial support of CXC grant GO0-1041X (WNB, NSS) and Smithsonian Astrophysical Observatory contract SV1-61010 for the CXC (NSS).

## REFERENCES

- Balbus, S. A. & Hawley, J. F. 1998, *Reviews of Modern Physics*, 70, 1
- Bautista, M. A. & Kallman, T. R. 2000, *ApJ*, 544, 581
- Begelman, M. C. & Rees, M. J. 1984, *MNRAS*, 206, 209
- Begelman, M. C., McKee, C. F., & Shields, G. A. 1983, *ApJ*, 271, 70
- Blandford, R. D. & Znajek, R. L. 1977, *MNRAS*, 179, 433
- Blundell, K. M., Mioduszewski, A. J., Muxlow, T. W. B., Podsiadlowski, P., & Rupen, M. P. 2001, *ApJ*, 562, L79
- Blustin, A. J., Page, M. J., Fuerst, S. V., Branduardi-Raymont, G., Ashton, C. E. 2005, *A&A*, 431, 111
- Boutloukos, S.; van der Klis, M.; Altamirano, D.; Klein-Wolt, M.; Wijnands, R.; Jonker, P. G.; Fender, R. P. 2006, *ApJ*, 653, 1435
- Brandt, W.N., Fabian, A.C., Dotani, T., Nagase, F., Inoue, H., Kotani, T., & Segawa, Y. 1996, *MNRAS*, 283, 1071
- Brandt, W.N. & Schulz, N.S. 2000, *ApJ*, 544, L123
- Canizares, C. R., Davis, J. E., Dewey, D., Flanagan, K. A., Galton, E. B., Huenemoerder, D. P., Ishibashi, K., Markert, T. H., Marshall, H. L., McGuirk, M., Schattenburg, M. L., Schulz, N. S., Smith, H. I., & Wise, M. 2005, *PASP*, 117, 1144
- Case, G.L., & Bhattacharya, D., 1998, *ApJ*, 504, 761
- Cottam, J., Sako, M., Kahn, S. M., Paerels, F., Liedahl, D. A. 2001, *ApJ*, 557, 101
- Davis, J. E. 2001, *ApJ*, 562, 575
- Ding, G. Q.; Qu, J. L.; Li, T. P. 2006, *AJ*, 131, 1693
- Fender, R., Spencer, R., Tzioumis, T., Wu, K., van der Klis, M., van Paradijs, J., & Johnston, H. 1998, *ApJ*, 506, L121
- Fender, R., Wu, K., Johnston, H., Tzioumis, T., Jonker, P., Spencer, R., van der Klis, M. 2004, *Nature*, 427, 222
- Fender, R., Belloni, T. M., & Gallo E. 2004, *MNRAS*, 355, 1105
- Frank, J., King, A. R., & Raine, D. J. 1992, *Accretion Power in Astrophysics* (2nd ed.; New York, Cambridge Univ. Press)
- Glass, I.S. 1994, *MNRAS*, 268, 742
- Galloway, D., Schulz, N. S., & Brandt, W. N. 2007, *ApJ*, submitted
- Grevesse, N.; Sauval, A. J. 1999, *A&A*, 347, 348
- Hasinger, G.; van der Klis, M. 1989, *A&A*, 225, 79
- Heinz, S., Schulz, N. S., Galloway, D., & Brandt, W. N. 2007, *ApJ*, in press
- Halpern, J. P. 1984, *ApJ*, 281, 90
- Houck, J. C. & Denicola, L. A. 2000, *ASP Conf. Ser.* 216: *Astronomical Data Analysis Software and Systems IX*, p. 591
- Iaria, R., Span, M., Di Salvo, T., Robba, N. R., Burderi, L., Fender, R., van der Klis, M., Frontera, F. 2005, *ApJ*, 619, 503
- Ji, L., Schulz, N. S., Nowak, M. & Marshall, H. L. 2007, *ApJ*, in prep.
- Jimenez-Garate, M. A., Raymond, J. C. & Liedahl, D. A. 2002, *ApJ*, 581, 1297
- Jimenez-Garate, M. A., Schulz, N. S., & Marshall, H. L. 2003, *ApJ*, 590, 432
- Jimenez-Garate, M. A., Raymond, J. C., Liedahl, D. A., & Hailey, C. J. 2005, *ApJ*, 625, 931
- Johnston, H.M., Wu, K., Fender, R., & Cullen, J.G. 2001, *MNRAS*, 328, 1193
- Jonker, P. G.; Swank, J. H.; Kuiper, L.; Homan, J.; Markwardt, C. B. 2006, *The Astronomer's Telegram*, 812, 1
- Jonker, P. G., Nelemans, G., & Bassa, C. G. 2007, *MNRAS*, 374, 999
- Juett, A. M., Schulz, N. S., & Chakrabarty, D. 2004, *ApJ*, 612, 308
- Juett, A. M., Schulz, N. S., Chakrabarty, D., Gorczyca, T. W. 2006, *ApJ*, 648, 1066
- Kallman, T., & White, N. E. 1989, *ApJ*, 341, 955
- Kallman, T.R., & Bautista, M. 2001, *ApJS*, 133, 221
- Kallman, T. R., Angelini, L., Boroson, B., & Cottam, J. 2003, *ApJ*, 583, 861
- Kallman, T. R., Palmeri, P., Bautista, M. A., Mendoza, C., Krolik, J. H., 2004, *ApJS*, 155, 675
- Kallman, T. R. & Palmeri, P. 2007, *Reviews of Modern Physics*, 79, 79
- Kaluzański, L.J., Holt, S.S., Boldt, E.A., & Serlemitsos, P.J. 1976, *ApJ*, 208, L71

- Kaspi, S., Brandt, W. N., George, I. M., Netzer, H., Crenshaw, D. M., Gabel, J. R., Hamann, F. W., Kaiser, M. E., Koratkar, A., Kraemer, S. B., Kriss, G. A., Mathur, S., Mushotzky, R. F., Nandra, K., Peterson, B. M., Shields, J. C., Turner, T. J., Zheng, W. 2002, *ApJ*, 574, 643
- Ko, Y.-K., & Kallman, T. R. 1994, *ApJ*, 431, 273
- Krauss, M. I., Schulz, N. S., Chakrabarty, D., Juett, A. M., Cottam, J. 2007, *ApJ*, 660, 605
- Krolik, J.H., Hawley, J.F., & Hirose, S. 2007, *Rev. Mex. Astron. Astrophys.*, 27, 1
- Kuster, M., Wilms, J., Stauber, R., Heindl, W. A., Rothschild, R. E., Shakura, N. I. & Postnov, K. A. 2005, *A&A*, 443, 753
- Lee, J.C., Reynolds, C.S., Remillard, R., Schulz, N.S., Blackman, E.G., & Fabian, A.C. 2001, *ApJ*, 567, 1102
- Liedahl, D. A. 1998, in *Lecture Notes in Phys.* 520, X-ray Spectroscopy in Astrophysics, ed. J. van Paradijs & J. A. M. Bleeker (Berlin, Springer), pp. 189
- London, R. A., 1982, in *Cataclysmic Variables and Low Mass X-ray Binaries*, ed. J. Patterson and D. Lamb, (Dordrecht: Reidel) p. 121
- Lynden-Bell, D. 1978, *Phys. Scripta*, 17, 185
- Margon, B., Lampton, M., Bowyer, S., & Cruddace, R. 1971, *ApJ*, 169, L23
- Markoff, S., Nowak, M. A., & Wilms, J. 2005, *ApJ*, 635, 1203
- Merloni, A. & Fabian, A.C. 2002, *MNRAS*, 332, 165
- Merloni, A. & Nayakshin, S. 2006, *MNRAS*, 372, 728
- Mignani, R., Caraveo, P.A., & Bignami, G.F. 1997, *A&A*, 474, 51
- Miller, J. M., Raymond, J., Fabian, A. C., Homan, J., Nowak, M., Wijnands, R., van der Klis et al. 2006, *Nature*, 441, 953
- Miller, J. M., Raymond, J., Homan, J., Fabian, A. C., Steeghs, D., Wijnands, R., Rupen, M., Charles, P., van der Klis, M., Lewin, W. H. G. 2006, *ApJ*, 646, 394
- Miller, J. M., Homan, J., Steeghs, D., Rupen, M., Hunstead, R. W., Wijnands, R., Charles, P. A., Fabian, A. C. 2006, *ApJ*, 653, 525
- Miller, J. M., Raymond, J., Fabian, A. C., Steeghs, D., Homan, J., Reynolds, C., van der Klis, M., Wijnands, R. 2006, *Nature*, 441, 953
- Mirabel, I.F. 2001, *Ap&SS*, 276, 319
- Moneti, A. 1992, *A&A*, 260, L7
- Morrison, R., & McCammon, D. 1983, *ApJ*, 278, 1082
- Muno, M. P., Lu, J. R., Baganoff, F. K., Brandt, W. N., Garmire, G.P. et al. 2005, *ApJ*, 633, 228
- Ostriker, E. C., McKee, C. F., & Klein, R. I. 1991, *ApJ*, 377, 593
- Parkinson, P. M. S., Tournear, D. M., Bloom, E. D., Focke, W. B., Reilly, K. T., Wood, K. S., Ray, P. S., Wolff, M. T., Scargle, Jeffrey D. 2003, *ApJ*, 595, 333
- Paerels F., Brinkman, A. C., van der Meer, R. L., Kaastra, J. S., Kuulkers, E., Boggende, A. F. den, Predehl, P., Drake, J. J., Kahn, S. M., Savin, D. W., and McLaughlin, B. M., 2001, *ApJ*, 546, 338
- Porquet, D. & Dubau, J. 2000, *A&AS*, 143, 495
- Predehl, P., & Schmitt, J. H. M. M., 1995, *A&A*, 293, 889
- Qu, J. L., Yu, W., & Li, T. P. 2001, *ApJ*, 7
- Różańska, A., Dumont, A.-M., Czerny, B., & Collin, S. 2002, *MNRAS*, 332, 799
- Schulz, N. S.; Hasinger, G.; Trümper, J. 1989, *A&A*, 225, 48
- Schulz, N.S., Chakrabarty, D., Marshall, H.L., Canizares, C.R., Lee, J.C., & Houck, J. 2001, *ApJ*, 563, 941
- Schulz, N. S. & Brandt, W. N. *ApJ*, 572, 971
- Schulz, N. S.; Cui, W.; Canizares, C. R.; Marshall, H. L.; Lee, J. C.; Miller, J. M.; Lewin, W. H. G. 2002, *ApJ*, 565, 1141
- Schulz, N. S.; Brandt, W. N.; Galloway, D. K.; Chakrabarty, D.; Heinz, S. 2006, in the Proceedings of the "The X-ray Universe 2005", ed. A. Wilson, ESA SP-604, Volume 1, Noordwijk: ESA Publications Division, pp. 201
- Shakura, N. I. & Sunyaev, R. A. 1973, *A&A*, 24, 337
- Shirey, R.E., Levine, A.M., & Bradt, H.V. 1999, *ApJ*, 524, 1048
- Stewart, R.T., Caswell, J.L., Haynes R.F., & Nelson, G.J. 1993, *MNRAS*, 261, 593
- Tarter, C. B., Tucker, W. H. & Salpeter, E. E. 1969, *ApJ*, 156, 943
- Tauris, T.M., Fender, R.P., van den Heuvel, E.P.J., Johnston, H.M., & Wu, K. 1999, *MNRAS*, 310, 1165
- Tennant, A.F., Fabian, A.C., & Shafer, R.A. 1986, *MNRAS*, 221, 27
- Vrtilek, S. D., Raymond, J. C., Garcia, M. R., Verbunt, F., Hasinger, G., Kürster, M. 1990, *A&A*, 235, 162
- Watanabe, S., Sako, M., Ishida, M., Ishisaki, Y., Kahn, S. M., Kohmura, T., Morita, U., Nagase, F., Paerels, F., Takahashi, T. 2003, *ApJ*, 597, L37
- Whelan, J.A.J., et al. 1977, *MNRAS*, 181, 259
- Wilms, J., Allen, A., & McCray, R. 2000, *ApJ*, 542, 914